Advances in Social Science, Education and Humanities Research, volume 196
2nd International Conference on Social Science, Public Health and Education (SSPHE 2018)

Cerebral Microbleeds Detection via Discrete Wavelet Transform and Back Propagation Neural Network

Jin Hong
School of Earth Sciences and Engineering
Sun Yat-Sen University
Guangzhou, China
hongj5@mail2.sysu.edu.cn

Zhi-Hai Lu*
School of Education Science
Nanjing Normal University
Nanjing, China
luzhihai@njnu.edu.cn

Abstract—Cerebral microbleeds (CMBs) are small perivascular hemosiderin deposits leaked through cerebral small vessels in normal or near normal tissue. The positions distribution of CMBs can indicate some underlying aetiologies. CMBs can be visualized by susceptibility-weighted imaging (SWI) which is high sensitivity to hemosiderin. In this paper, we proposed a hybrid method to detect the CMBs automatically. This method first applied discrete wavelet transform (DWT) to extract the features of the brain images, and then employed principal component analysis (PCA) to perform reduction of features. At last, the obtained features were inputted to back propagation shallow neural network (BPNN) with a single-hidden layer for training and prediction. K-fold cross validation was applied to avoid overfitting and evaluate the generalization ability of BPNN for selecting the best model. Based on this method, a good result was obtained with a sensitivity of 88.47± 0.96%, a specificity of 88.38± 1.00%, and an accuracy of 88.43± 0.97%, which is better than two state-of-the-art approaches.

Keywords—discrete wavelet transform, back propagation, shallow neural network, cerebral microbleeds

I. INTRODUCTION

With the improvement of medical technology, people's life span is also getting longer. This is not only due to the improvement of the technology for treating diseases but also due to the improvement of disease prevention technology. More and more researches show that there are relationships between cerebral microbleeds (CMBs) and intra-cerebral hemorrhage (ICH), which means CMBs can indicate some underlying aetiologies caused by ICH [1]. CMBs as a kind of subclinical sign can be detected in a few years before the onset of the disease, which provide an important reference for disease prevention [2].

CMBs are small perivascular hemosiderin deposits leaked through cerebral small vessels in normal or near normal tissue [3]. CMBs are visualized as small and rounded radiological entities by magnetic resonance imaging (MRI) due to the superparamagnetic of hemosiderin which lead to fast decay of signal. Developments in software and hardware of MRI have improved the capacity of identifying CMBs. Currently, susceptibility-weighted imaging (SWI) is more preferred to be employed to visualize CMBs because of its higher sensitivity to hemosiderin comparing to traditional T1 and T2 MRI. More and smaller CMBs can be recognized using SWI [4]. Therefore, the brain images of CMBs in this study are also scanned by this technique.

Traditionally, CMBs are detected manually by radiologists, which is laborious, unreproducible, time-consuming, and error-prone. The high intra-observer and inter-observer variability would cause different results of CMBs detection every time. Both small CMBs, which would be ignored easily, and CMB mimics, which would confuse the observer, can cause the error results of CMBs detection. Hence it is necessary to develop automatic techniques for detecting CMBs.

Many researchers tried to explore the best means to detect CMBs automatically, accurately and rapidly. Some advances have been obtained in last decade, particularly in the field of image processing [5-7] in medical image analysis. [8] developed an automated segmentation technique for microbleed detection. [9] developed a novel multiple radial symmetry transform (MRST) and random forests (RF) method for detecting CMBs. [10] developed the radial symmetry transform (RST) to identify the possible CMBs. [11] proposed a method which can detect CMBs semi-automatically. 2D fast RST was applied to detect the putative CMBs firstly, and then the 3D region growing was employed to discard the falsely identified CMBs. [12] suggested a novel technique namely multi-scale Laplacian of Gaussian (MLG) to identify the possible CMBs. Then the CMB candidates were classified into two types (“definite” and “possible”) using a cascaded binary RF. [13] developed a two-step method to detect CMBs. They selected twelve features based on the nature properties of CMBs. Then random forest as a classifier was applied to recognize the CMB candidates’ location, and an object-based classifier would be used to eliminate the false CMBs according their locations.[2] proposed an artificial neural-network containing one single-hidden layer feedforward neural-network for CMBs detection. Tricks that leaky rectified linear unit (ReLU) and early stopping were employed in their study. [14] suggested a seven-layer deep neural network to detect CMBs based on sparse autoencoder. [15] developed convolutional neural network.[16] used wavelet entropy and naïve Bayesian classifier.

Above methods have achieved great improvements for detecting CMBs. To further explore the possibility of improving the accuracy of detecting CMBs, our team tried many methods and found an effective one which performed better than those state-of-the-art approaches based on traditional machine learning. Firstly, we used sliding neighborhood processing (SNP) technique to generate the input images and their target value. Then discrete wavelet transformation (DWT) was employed to extract the features of the input images. Afterwards, principal component analysis (PCA) was applied to reduce the features

and remove the possible correlated relationships between those features for avoiding the bias of prediction results. Finally, the features and their corresponding target values were sent to back propagation neural network (BPNN) for training and predicting.

II. MATERIALS

Ten patients diagnosed with cerebral microbleed and ten healthy controls (HCs) were enrolled. Syngo MR B17 software was employed to reconstruct the 3D SWI images. The size of the 3D SWI images are 364 × 448 × 48. Three neuron-radiologists with over twenty years of experience were employed to label the CMB voxels manually. In this study, both the voxels labelled "possible" and "definite" are considered as CMBs.

We used SNP technique to generate the input images and their target value. The size of sliding window is 7 × 7. The sliding window swept over twenty subjects and generated 68,847 CMB samples and 151,837,713 Non-CMB samples, more details about the procedure of generating the samples can be found in (Hou et al., 2017). In view of the imbalance of the samples, undersampling was used to remove the Non-CMBs randomly. Finally, 137,676 samples including 68,847 CMB samples and 68,829 Non-CMB samples were obtained.

III. METHODS

A. Discrete Wavelet Transformation

Discrete wavelet transformation (DWT) as an important means in signal processing has a critical advantage comparing to Fourier transforms: it can obtain both frequency and location information. It is available to obtain temporal resolution in multiple scale for DWT with this advantage[17-20]. The multiple scale information can be represented by a set of wavelet coefficients, and the wavelet coefficients are derived from decomposing the signal. Furthermore, wavelet coefficients can further be selected as features for classification.

Suppose there is a signal x, the scaling and translation parameters are m^i and jnm^i where m and n are unchanged, and their values are greater than 1 and 0 respectively. i and j are integers. The expression of DWT is as follows:

$$\mathrm{W[i,j]} = \frac{1}{m^{i/2}} \sum_{t=-\infty}^{+\infty} x[t]\varphi\left(\frac{t - m^i jn}{m^i}\right) \quad (1)$$

where φ denotes the wavelet function, x[t] denotes the discretized signal function.

It is worth noting that the values of m and n are selected to make the mother wavelets form an orthonormal basis. It is practical to choose 2 and 1 as the values of m and n respectively for satisfying this condition. Afterwards, DWT can be implemented using filter blank methods when the coefficients can be considered as a filter [21]:

$$\mathrm{W}(i,j) = \sum_{t=0}^{L-1} x(t)(2^{-i/2})\varphi(2^{-i}t - j) \quad (2)$$

The meaningful of DWT is to decompose the original signal into multiple level coefficients. The method of decomposing signal developed by [22] can convert the signal to a series of coefficients including approximation and detail components in multiple level. The procedure of decomposing is shown in Fig. 1, *h(n)* and *g(n)* denote the low pass filter and the high pass filter respectively; *A(L)* and *D(L)* denote the approximation and detail coefficients of level L respectively, and the L is given according the specific situation. Approximation and detail coefficients are obtained after that signal is passed through *h(n)* and *g(n)* and downsampled which is used to maintain the length of the signal. Hence the approximation and detail coefficients represent the low and high frequency information of the signal respectively [23-26].

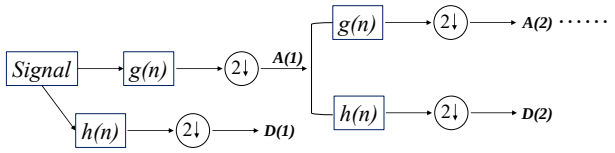

Fig. 1. Wavelet decomposition tree

B. Principal Component Analysis

Our goal is to classify the CMBs using those coefficients as the features of classification. Nevertheless, it is possible that some coefficients are correlated which can lead to bias of the prediction results and some coefficients are redundant which can make noise [27, 28].

PCA invented by [29] is a statistical technique for data analysis and processing. It converts the variables that possibly correlated to principal components that linearly uncorrelated using an orthogonal transformation. The principal components transformed by PCA sorted by variance. The first principal component has the largest possible variance and the second one has the second largest variance, and so on. Generally, the larger variance that the component has, the more important information that it has. Hence the PCA can perform reduction of variables by retaining a part of principal components that have larger possible variance and ignoring the rest part. The retained principal components contain most of the information of the original data set, and the relationships between the principal components are uncorrelated.

Consider a series of k-dimensional data vectors {xn} [30] which have been normalized, n ∈ [1, 2, ……, N]. The sample covariance matrix is calculated as $\boldsymbol{C} = \sum_n (\boldsymbol{x}_n - \overline{\boldsymbol{x}})(\boldsymbol{x}_n - \overline{\boldsymbol{x}})^{\mathrm{T}}/N$, where $\overline{\boldsymbol{x}}$ is the average value of samples. The eigenvalues and eigenvectors can be calculated according to the covariance matrix C. The eigenvalues are in one-to-one correspondence with the eigenvectors. The eigenvectors corresponding to the q largest eigenvalues are retained and defined as V= (v1, v2, …, vq). Finally, the q principal components are given as $\boldsymbol{p}_n = (\boldsymbol{x}_n - \overline{\boldsymbol{x}})\boldsymbol{V}^{\mathrm{T}}$. The principal components pj are uncorrelated and lesser than k in number generally.

C. Back Propagation Neural Network

Back propagation neural network (BPNN) as one kind of feed-forward neural-network is widely applied to pattern recognition, function approximation, classification, and so on [31-33].

BPNN was used as the classifier in this study. The features (namely principal components) derived from PCA were sent to

the neural network for training. The structure of BPNN contains input layer, hidden layer and output layer (Fig. 2). In this study, the number of the neurons in input layer is determined by the features, while that in hidden layer would be determined by grid searching method.

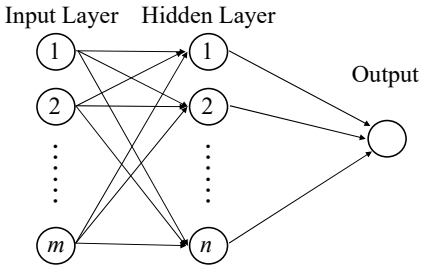

Fig. 2. A two-layer BPNN structure

Suppose the input is i and the target is j. The values of neurons in the hidden layer can be expressed as below:

$$g = f_H(w_H^{\mathrm{T}} i + b_H) \tag{3}$$

where f_H, w_H, and b_H are activation function, weights, and biases of hidden layer neurons, respectively. Then the values of neurons in output can be expressed as below:

$$k = f_O(w_O^{\mathrm{T}} g + b_O) \tag{4}$$

where f_O, w_O, and b_O are activation function, weights, and biases of output neurons, respectively. It is worth noting that all of the weights and biases derived from learning via back propagation. Scaled conjugate gradient (SCG) method [34-36] was employed for training the BPNN. The activation functions need to be given before training. Sigmoid function was selected as the activation functions of hidden layer neurons and output neurons in this study.

D. K-fold Cross Validation

K-fold cross validation was applied to evaluate the generalization ability of BPNN for selecting the best model. The samples were randomly divided into K folds and each fold substantially contains the same number of samples. Then K-1 folds were used as the training samples and the rest one-fold was used as the test samples at every run. K runs were implemented [37, 38]. Finally, K test errors would be obtained, and their average value is the overall error of the model. In this study, the samples were divided into ten folds (K was set to 10), and the cross-validation procedure is shown in Fig. 3.

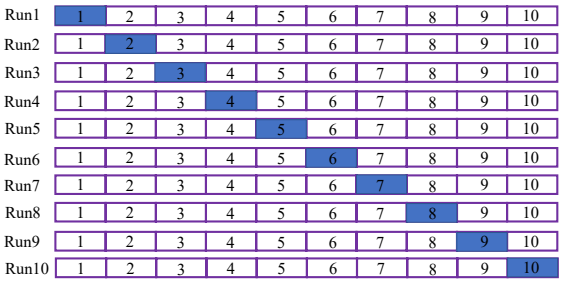

Fig. 3. K-fold cross validation workflow

E. Evaluation

Three statistical indicators were applied to evaluate the performance of our method. They are sensitivity, specificity and accuracy, and they defined as below:

$$\text{Sensitivity} = \text{TP} / (\text{TP} + \text{FN}) \tag{5}$$

$$\text{Specificity} = \text{TN} / (\text{TN} + \text{FP}) \tag{6}$$

$$\text{Accuracy} = (\text{TP} + \text{TN}) / (\text{TP} + \text{FN} + \text{TN} + \text{FP}) \tag{7}$$

TP represents a CMB voxel classified correctly, TN represents a Non-CMB voxel classified correctly, FP represents a Non-CMB voxel incorrectly classified as CMB, FN represents a CMB voxel incorrectly classified as Non-CMB.

IV. Results

The hyperparameters of our method was tuned by either trial-and-error or grid search method. We finally set those hyperparameters in Table I.

TABLE I. HYPERPARAMETER SETTING OF OUR METHOD

Wavelet Name	Db3
Wavelet decomposition	4-level
PCA threshold	98%
# hidden neurons	12
Activation function	Sigmoid
Neural network training method	Scaled conjugate gradient

The results over 10x10-fold cross validation was shown below in Table II and Fig. 4. Here we obtained a sensitivity of 88.47± 0.96%, a specificity of 88.38± 1.00%, and an accuracy of 88.43± 0.97%.

TABLE II. STATISTICAL RESULT OF OUR METHOD

Run	Sensitivity (%)	Specificity (%)	Accuracy (%)
1	87.31	86.96	87.14
2	87.35	87.63	87.49
3	89.73	89.59	89.66
4	89.91	89.83	89.87
5	89.22	89.29	89.26
6	88.20	87.97	88.08
7	88.21	88.26	88.24
8	88.64	88.56	88.60
9	88.74	88.66	88.70
10	87.40	87.08	87.24
Average	88.47± 0.96	88.38± 1.00	88.43± 0.97

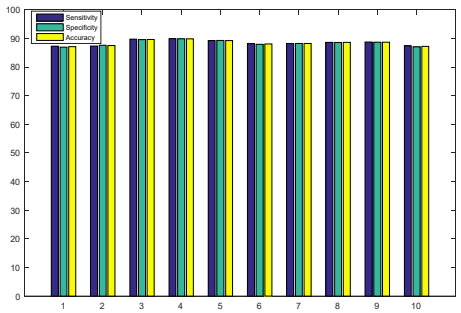

Fig. 4. Statistical of our method

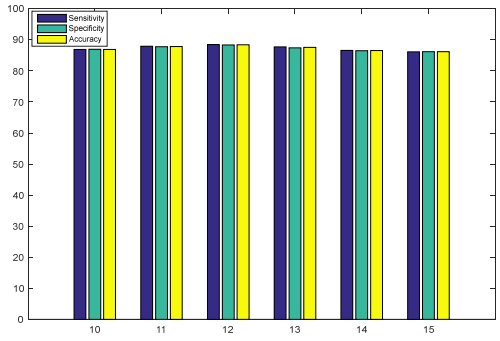

Fig. 5. Performance against number of hidden neurons

We used grid search to check the optimal number of hidden neurons of this back-propagation neural network. Suppose *n* represents the number of hidden neurons, and we vary *n* from 10 to 15. The results are shown in Table III and Fig. 5, where the best results were highlighted in bold.

TABLE III. PERFORMANCE AGAINST NUMBER OF HIDDEN NEURONS

Value of *n*	Sensitivity (%)	Specificity (%)	Accuracy (%)
10	86.94± 1.22	86.97± 1.06	86.95± 1.14
11	87.96± 0.45	87.80± 0.57	87.88± 0.50
12	**88.47± 0.96**	**88.38± 1.00**	**88.43± 0.97**
13	87.75± 0.86	87.46± 1.11	87.61± 0.96
14	86.61± 0.90	86.51± 1.11	86.56± 1.00
15	86.17± 1.07	86.22± 1.26	86.20± 1.15

Finally, we compared our method with two state-of-the-art approaches: (i) random forest (RF) [9]; and (ii) wavelet entropy and naïve Bayesian classifier [16]. The results are shown in Table IV.

TABLE IV. COMPARISON TO STATE-OF-THE-ART APPROACHES

Method	Sensitivity(%)	Specificity(%)	Accuracy(%)
RF [9]	85.7%	99.5%	Not available
WE-RBF [16]	76.90	76.91	76.90
Proposed	88.47± 0.96	88.38± 1.00	88.43± 0.97

V. CONCLUSIONS

In this paper, a hybrid method was developed to detect cerebral microbleeds. Compared to two state-of-the-art approaches, the result of this method achieved a better performance with a sensitivity of 88.47± 0.96%, a specificity of 88.38± 1.00%, and an accuracy of 88.43± 0.97%. Future work should focus on collecting more brain images.

REFERENCES

[1] A. Charidimou and DJ. Werring, "Cerebral microbleeds: Detection, mechanisms and clinical challenges," Future Neurology, vol. 6, no. 5, pp. 587-611, 2011.

[2] Y.-D. Zhang, X.-X. Hou, Y. Chen, H. Chen, M. Yang, J. Yang, et al., "Voxelwise detection of cerebral microbleed in CADASIL patients by leaky rectified linear unit and early stopping," Multimedia Tools and Applications, vol. 77, no. 17, pp. 21825-21845, September 2018.

[3] S.M Greenberg, M.W Vernooij, C. Cordonnier, A. Viswanathan, R. Al-Shahi Salman, S. Warach, et al., "Cerebral microbleeds: a guide to detection and interpretation," The Lancet Neurology, vol. 8, no. 2, pp. 165-174, February 2009.

[4] R. Nandigam, A. Viswanathan, P. Delgado, M. Skehan, E. Smith, J. Rosand, S. Greenberg, et al., "MR imaging detection of cerebral microbleeds: effect of susceptibility-weighted imaging, section thickness, and field strength," Ajnr Am J Neuroradiol, vol. 30, no. 2, pp. 338-43, 2009.

[5] Y. Zhang, Z. Dong, L. Wu, and S. Wang, "A hybrid method for MRI brain image classification," Expert Systems with Applications, vol. 38, no. 8, pp. 10049-10053, 2011.

[6] Y.-D. Zhang and L. Wu, "An Mr Brain Images Classifier via Principal Component Analysis and Kernel Support Vector Machine," Progress In Electromagnetics Research, vol. 130, 369-388, 2012.

[7] Y. Zhang, B. Peterson, Z. Dong, "A support-based reconstruction for SENSE MRI," Sensors, vol. 13, no. 4, pp. 4029-4040, 2013.

[8] M.L. Seghier, M.A. Kolanko, A.P. Leff, H.R. Jäger, S.M. Gregoire, D.J. Werring, "Microbleed Detection Using Automated Segmentation (MIDAS): A New Method Applicable to Standard Clinical MR Images," PLOS ONE, vol. 6, no. 3, pp. e17547, 2011

[9] S. Roy, A. Jog, E. Magrath, J.A. Butman, D.L. Pham, "Cerebral Microbleed Segmentation from Susceptibility Weighted Images," Proceedings of SPIE. 9413: Article ID. 94131E, 2015

[10] H.J. Kuijf, J. de Bresser, M.I. Geerlings, M.M.A. Conijn, M.A. Viergever, G.J. Biessels, et al., "Efficient detection of cerebral microbleeds on 7.0T MR images using the radial symmetry transform," NeuroImage, vol. 59, no. 3, pp. 2266-73, February 2012

[11] W. Bian, C.P. Hess, S.M. Chang, S.J. Nelson, J.M. Lupo, "Computer-aided detection of radiation-induced cerebral microbleeds on susceptibility-weighted MR images," NeuroImage Clinical, vol. 2, pp. 282-290, 2013

[12] A. Fazlollahi, F. Meriaudeau, L. Giancardo, V.L. Villemagne, C.C. Rowe, P. Yates, et al., "Computer-aided detection of cerebral microbleeds in susceptibility-weighted imaging," Comput Med Imaging Graph, vol. 46, no. 3, pp. 269-276, December 2015

[13] K. Standvoss, T. Crijns, L. Goerke, D. Janssen, S. Kern, T. Niedek, et al., "Cerebral Microbleed Detection in Traumatic Brain Injury Patients using 3D Convolutional Neural Networks," Conference on Medical Imaging - Computer-Aided Diagnosis, 10575: Article ID. UNSP 105751D, 2018

[14] Y.-D. Zhang, Y. Zhang, X.-X. Hou, H. Chen, S.-H. Wang, "Seven-layer deep neural network based on sparse autoencoder for voxelwise detection of cerebral microbleed," Multimedia Tools and Applications, vol. 77, no. 9, pp. 10521-10538, May 2018.

[15] S. Wang, Y. Jiang, X. Hou, H. Cheng, S. Du, "Cerebral Micro-Bleed Detection Based on the Convolution Neural Network With Rank Based Average Pooling," IEEE Access, vol. 5, pp. 16576-16583, 2017

[16] H.-n. Wang and B. Gagnon, "Cerebral microbleed detection by wavelet entropy and naive Bayes classifier," Advances in Biological Sciences Research, vol. 4, pp. 507-510, 2017.

[17] S.-H. Wang, Y. Zhang, Y.-J. Li, W.-J. Jia, F.-Y. Liu, M.-M. Yang, et al., "Single slice based detection for Alzheimer's disease via wavelet entropy and multilayer perceptron trained by biogeography-based optimization," Multimedia Tools and Applications, vol. 77, no. 9, pp. 10393-10417, May 2018.

[18] S.H. Wang, K. Muhammad, Y. Lv, Y. Sui, L. Han, Y.D. Zhang, "Identification of Alcoholism based on wavelet Renyi entropy and three-segment encoded Jaya algorithm," Complexity, Article ID: 3198184, 2018.

[19] S.-H. Wang, P. Phillips, Z.-C. Dong, Y.-D. Zhang, "Intelligent facial emotion recognition based on stationary wavelet entropy and Jaya algorithm," Neurocomputing, vol. 272, pp. 668-676, January 2018.

[20] S. Wang, P. Li, P. Chen, Phillips P., G. Liu, S. Du, et al., "Pathological Brain Detection via Wavelet Packet Tsallis Entropy and Real-Coded Biogeography-based Optimization," Fundamenta Informaticae, vol. 151, no. 1-4, pp. 275-91, 2017.

[21] K.L. Butler-Purry and M. Bagriyanik , "Characterization of transients in transformers using discrete wavelet transforms," IEEE Transactions on Power Systems, vol. 18, no. 2, pp. 648-56, 2003.

[22] D. Bianchi, E. Mayrhofer, M. Gröschl, G. Betz, A. Vernes, "Wavelet packet transform for detection of single events in acoustic emission

signals," Mechanical Systems & Signal Processing, vol. 64-65, pp. 441-51, 2015.

[23] S. Wang, Y. Li, Y. Shao, C. Cattani, S. Du, "Detection of Dendritic Spines using Wavelet Packet Entropy and Fuzzy Support Vector Machine," Cns Neurol Disord Drug Targets, vol. 16, no. 2, pp. 116-121, 2017.

[24] Y. Zhang, D.R. Nayak, M. Yang, Y. Shao, B. Liu, S. Wang, "Detection of unilateral hearing loss by Stationary Wavelet Entropy," Cns & Neurological Disorders Drug Targets, vol. 16, no. 2, pp. 15-24, 2016

[25] Y.D. Zhang, Z.J. Yang, H.M. Lu, X.X. Zhou, P. Phillips, Q.M. Liu, et al., "Facial Emotion Recognition based on Biorthogonal Wavelet Entropy, Fuzzy Support Vector Machine, and Stratified Cross Validation," IEEE Access, vol. 4, no. 99, pp. 8375-8385, 2017.

[26] S. Wang, M. Yang, S. Du, J. Yang, B. Liu, J.M. Gorriz, et al., "Wavelet entropy and directed acyclic graph support vector machine for detection of patients with unilateral hearing loss in MRI scanning," Frontiers in Computational Neuroscience, 10: Article ID. 160, 2016.

[27] Y. Zhang, S. Lu, X. Zhou, M. Yang, L. Wu, B. Liu, et al., "Comparison of machine learning methods for stationary wavelet entropy-based multiple sclerosis detection: decision tree, k-nearest neighbors, and support vector machine," Simulation, vol. 92, no. 9, pp. 861-871, 2016.

[28] S. Wang, M. Yang, B. Liu, J. Yang, P. Chen, X. Zhou, et al., "Computer-aided detection of left and right sensorineural hearing loss by wavelet packet decomposition and least-square support vector machine." Journal of the American Geriatrics Society, vol. 64, no. S2, Article ID: S350, 2016.

[29] K. Pearson, "LIII. On lines and planes of closest fit to systems of points in space," The London, Edinburgh, and Dublin Philosophical Magazine and Journal of Science, vol. 2, no. 11, pp. 559-572, 1901.

[30] J. Pietschnig, L. Schröder, I. Ratheiser, I. Kryspin-Exner, M. Pflüger, D. Moser, et al., "Facial emotion recognition and its relationship to cognition and depressive symptoms in patients with Parkinson's disease," International psychogeriatrics, vol. 28, no. 7, pp. 1165-79, 2016.

[31] Y.-D. Zhang, C. Pan, J. Sun, C. Tang, "Multiple sclerosis identification by convolutional neural network with dropout and parametric ReLU," Journal of computational science, vol. 28, pp. 1-10, 2018

[32] Y.-D. Zhang, C. Pan, X. Chen, F. Wang, "Abnormal breast identification by nine-layer convolutional neural network with parametric rectified linear unit and rank-based stochastic pooling," Journal of Computational Science, vol. 27, pp. 57-68, 2018.

[33] S.-H. Wang, H. Cheng, P. Phillips, Y.-D. Zhang, "Multiple Sclerosis Identification Based on Fractional Fourier Entropy and a Modified Jaya Algorithm," Entropy, vol. 20, no. 4, pp. 254, 2018.

[34] S.-H. Wang, Y.-D. Lv, Y. Sui, S. Liu, S.-J. Wang, Y.-D.Zhang, "Alcoholism detection by data augmentation and convolutional neural network with stochastic pooling," Journal of medical systems, vol. 42, no. 1, pp. 2, 2018.

[35] Y.-D. Zhang, Y. Zhang, P. Phillips, Z. Dong, S. Wang, "Synthetic minority oversampling technique and fractal dimension for identifying multiple sclerosis," Fractals, vol. 25, no. 04, pp. 1740010, 2017.

[36] S. Wang, M. Yang, J. Li, X. Wu, H. Wang, B. Liu, et al., "Texture analysis method based on fractional Fourier entropy and fitness-scaling adaptive genetic algorithm for detecting left-sided and right-sided sensorineural hearing loss," Fundamenta Informaticae, vol. 151, no. 1-4, pp. 505-21, 2017.

[37] Y. Zhang, S. Wang, Z. Dong, "Classification of Alzheimer disease based on structural magnetic resonance imaging by kernel support vector machine decision tree," Progress In Electromagnetics Research, vol. 144, pp. 171-84, 2014.

[38] Y. Zhang, S. Wang, Z. Dong, P. Phillip, G. Ji, J. Yang, "Pathological brain detection in magnetic resonance imaging scanning by wavelet entropy and hybridization of biogeography-based optimization and particle swarm optimization," Progress In Electromagnetics Research, vol. 152, pp. 41-58, 2015.